

Published in final edited form as:

Cancer Res. 2008 August 15; 68(16): 6608–6616. doi:10.1158/0008-5472.CAN-08-1117.

K-Ras Nanoclustering is Subverted by Over-expression of the Scaffold Protein Galectin-3

Ruby Shalom-F Feuerstein^{1,4}, Sarah J. Plowman^{2,4}, Barak Rotblat¹, Nicholas Ariotti², Tianhai Tian^{2,3}, John F. Hancock^{2,*}, and Yoel Kloog^{1,*}

¹ Department of Neurobiology, The George S. Wise Faculty of Life Sciences, Tel Aviv University, Tel Aviv, Israel.

² Institute for Molecular Bioscience, University of Queensland, Brisbane 4072, Australia.

Abstract

The spatial organization of K-Ras proteins into nanoclusters on the plasma membrane is essential for high fidelity signal transduction. The mechanism underlying K-Ras nanoclustering is unknown. We show here that K-Ras.GTP recruits Galectin-3 (Gal-3) from the cytosol to the plasma membrane where it becomes an integral nanocluster component. Importantly we demonstrate that the cytosolic level of Gal-3 determines the magnitude of K-Ras.GTP nanoclustering and signal output. The β -sheet layers of the Gal-3 carbohydrate recognition domain (CRD) contain a hydrophobic pocket that may accommodate the farnesyl group of K-Ras. V125A substitution within this hydrophobic pocket yields a dominant negative Gal-3(V125A) mutant that inhibits K-Ras activity. Gal-3(V125A) interaction with K-Ras.GTP, reduces K-Ras.GTP nanocluster formation, which abrogates signal output from the Raf/MEK/ERK pathway. Gal-3(V125A) negatively regulates cell growth and reduces cellular transformation. Thus regulation of K-Ras nanocluster formation and signal output by Gal-3 critically depends on the integrity of the Gal-3 hydrophobic pocket. These results show that Gal-3 over-expression in breast cancer cells, which increases K-Ras signal output represents oncogenic subversion of plasma membrane nanostructure.

Keywords

cell transformation; Galectin-3; Galectin-3(V125A); K-Ras; nanoclusters

Introduction

Cell fate decisions are regulated by the magnitude and duration of a given stimulus. To maintain tissue homeostasis individual cells within the tissue must respond in concert to a given strength of signal input with a defined strength of signal output for a discrete period of time. Loss of cellular responsiveness to these cues leads to aberrant cell growth and tumour formation. One of the key regulators of intracellular signal transduction is the Ras family of proteins. Ras proteins are guanine nucleotide binding proteins that act as molecular switches on the inner plasma membrane. In response to growth factor receptor activation, Ras proteins are activated by guanine nucleotide exchange factors that stimulate GDP/GTP exchange. In the active GTP-bound state, Ras proteins recruit downstream effectors from the cytosol to the plasma

* Corresponding Authors: Yoel Kloog: kloog@post.tau.ac.il Department of Neurobiology, The George S. Wise Faculty of Life Sciences, Tel Aviv University, Tel Aviv, 69978 Israel. John F Hancock: j.hancock@imb.uq.edu.au Institute for Molecular Bioscience, University of Queensland, Brisbane 4072, Australia.

³present address, Department of Mathematics, University of Glasgow, Glasgow, UK.

⁴these authors contributed equally

membrane for activation. Ras proteins are positioned at the junction between cell surface receptors and a number of intracellular signalling cascades, such as the Raf/MEK/ERK, PI-3K/Akt and RalGDS pathways. Therefore in response to extracellular stimuli, Ras proteins can induce a range of cellular responses including proliferation, differentiation and apoptosis by orchestrating the activation of specific intracellular signal transduction cascades (1-3). Approximately 15% of human malignancies express mutant Ras proteins that are constitutively GTP-loaded and unresponsive to extracellular stimuli, these oncogenic mutations are particularly prevalent in the *K-ras* gene and are associated with colon, lung and pancreatic cancer (4).

To regulate signal transmission from cell surface receptors to intracellular signalling cascades K-Ras must be localized to the plasma membrane (5). The specific motifs that target K-Ras to the plasma membrane are encoded by the C-terminal hypervariable region (HVR) and include a farnesylated cysteine residue and a polybasic domain composed of six contiguous lysine residues (5). Spatial analysis shows that K-Ras exhibits non-random distribution on the inner leaflet of the plasma membrane (6-9). Approximately 40% of K-Ras proteins are organized into nanoclusters of ~7 proteins with radii of ~9nm. The remaining ~60% of K-Ras proteins are arrayed as monomers (7). The non-random organization of K-Ras.GTP has important functional implications since abrogation of K-Ras.GTP nanoclustering inhibits signal transmission to downstream effectors (10). Importantly, the cytosolic effector Raf-1 is recruited to the plasma membrane by K-Ras.GTP proteins resident in nanoclusters but not by K-Ras.GTP monomers, demonstrating that the K-Ras.GTP nanocluster acts as a platform to which downstream effectors are recruited (10).

We have recently demonstrated that the organization of K-Ras.GTP into nanoclusters provides a mechanism by which high fidelity signal transmission across the plasma membrane can be achieved (10). Central to this signal transmission mechanism is the fixed ratio of K-Ras.GTP proteins in nanoclusters to K-Ras.GTP proteins diffusing as monomers that remains constant over a multi-log range of K-Ras.GTP levels (7). The fixed K-Ras.GTP clustered fraction results in a linear relationship between the number of K-Ras.GTP nanoclusters on the plasma membrane and the stimulating epidermal growth factor (EGF) concentration (7,10). How K-Ras.GTP nanoclustering is regulated and in particular how the clustered fraction is maintained is currently unknown.

Galectin-3 (Gal-3) is a β -galactoside binding protein that contains a C-terminal carbohydrate-recognition-binding domain and an N-terminal proline- and glycine-rich domain (11). Gal-3 exists as a cytosolic protein (12) but immuno-precipitation studies show that K-Ras and Gal-3 can directly interact if K-Ras is GTP-loaded and farnesylated (12). Expression of exogenous Gal-3 stabilizes K-Ras GTP-loading in response to EGF stimulation and regulates signal output (12,13). Taken together these data suggest that Gal-3 may regulate K-Ras.GTP nanocluster formation. Interestingly Gal-3 is highly expressed in a number of human malignancies and Gal-3 expression has been shown to stimulate cellular proliferation, anchorage independent cell growth and inhibition of apoptosis via K-Ras mediated Raf/MEK/ERK activation (13). How Gal-3 interacts with K-Ras.GTP and regulates signal output is currently unknown. However clues may be gained from studies performed to determine the mode of interaction of a related protein Galectin-1 with the H-Ras isoform. As with K-Ras.GTP and Gal-3, the interaction of H-Ras.GTP with Gal-1 is largely dependent on the farnesyl group of the H-Ras protein (14-16). Structural modeling of Gal-1 identified a putative farnesyl-binding pocket between the two β -sheet layers of the carbohydrate recognition domain (CRD) (14). Disruption of this putative prenyl-binding pocket by mutation of leucine 11 to alanine (Gal-1(L11A)), yields a dominant negative protein which inhibits the activation of H-Ras by EGF and signaling to ERK, and inhibits H-RasG12V transforming activity (14). Importantly structural modeling also identified a highly homologous putative prenyl-binding pocket in Gal-3 (16), suggesting

that Gal-3 may regulate K-Ras nanocluster formation in a manner analogous to H-Ras.GTP and Gal-1 (17).

Here we investigate the role of Gal-3 in K-Ras nanocluster formation and function using quantitative immuno-EM spatial mapping and FLIM-FRET microscopy. Using this method we demonstrate the Gal-3 is an integral component of the K-Ras.GTP but not the K-Ras.GDP nanocluster. Furthermore we show that the hydrophobic pocket in Gal-3 (16) critically mediates K-Ras.GTP nanocluster formation and signal output. The ability of Gal-3 to mediate K-Ras.GTP nanocluster formation is directly correlated with the level of signal output and the transformed phenotype of breast cancer cells. Together these data demonstrate the critical role of Gal-3 in controlling K-Ras signal output and tumorigenesis.

Materials and Methods

Cloning

The pcDNA3 Gal-3 (12) vector was used as a template for generating the Valine 125 to Alanine substitution using the Quickchange system (Promega). The construct was verified by sequencing. For protein expression, wild type and mutant Gal-3 were amplified by PCR reactions using forward (5'-CCATGGCAGACAATTTTCGCTCC-3') and reverse (5'-AAGCTTTTATATCATGGTATATGAAGC-3') primers. The PCR products were inserted into NcoI/HindIII sites of Pet 28a+ vector (Invitrogen). The GFP-K-Ras, GFP-K-RasG12V, anti-sense Gal-3 and anti-sense Gal-1 constructs have described previously (12,18). mRFP-Gal-3 was generated from pcDNA3 Gal-3 using an mRFP1 cDNA (19) kindly provided by Dr R.Tsien.

Protein purification

Bacteria transformed with Gal-3 and Gal-3(V125A) were grown over night at 18 °C. Bacterial pellets were re-suspended (with 500 ml TrisHCl pH 7.4 detergent free buffer), sonicated and then centrifuged for 10 minutes at 20800 ×g. The supernatant was loaded onto lactosylated Sepharose 4B as described (14). Fractions were collected and the presence of recombinant Gal-3 and Gal-3(V125A) was detected by western blotting using anti Gal-3 antibody.

Structural and sequence alignment

The sequences of Gal-1 and Gal-3 were aligned using the ClustalW algorithm⁵. The structures of Gal-1 and Gal-3 (PDB codes: 1SLA and 1A3K) were superimposed using the 'Magic Fit' function of the SwissPdb Viewer software (Guex, N. and Peitsch, M.C. (1997) SWISS-MODEL and the Swiss-PdbViewer: An environment for comparative protein modeling. *Electrophoresis* 18, 2714–2723⁶) and the structures were presented using the PyMol software⁷.

Cell culture and transfection

The human breast cancer cell lines BT-549, BT-549 stably expressing Gal-3 (BT-549/Gal-3) (13) and HEK 293 cells (18) were grown as described previously. BT-549 cells stably expressing pcDNA3/Gal-3(V125A) were established by selection with G418. HEK 293 cells were co-transfected (calcium phosphate method) with plasmids coding for Gal-3, Gal-3 (V125A), and GFP-K-RasG12V, and the appropriate vector controls. Cells were lysed 48 h after transfection in lysis buffers as detailed earlier (18).

⁵www.ebi.ac.uk/clustalw/

⁶<http://www.expasy.org/spdbv/>

⁷<http://www.pymol.org>

For immuno-EM BHK cells cultured as previously described (7).

Western immunoblotting

Cell lysates were subjected to SDS-PAGE, followed by immunoblotting with the following antibodies: pan-Ras (Ab-3) (Calbiochem, La Jolla, CA); anti-K-Ras, anti-tubulin, anti-phospho-ERK and anti-ERK (Sigma-Aldrich' St. Louis, MO); anti-Gal-3 (12); anti-GFP (Santa Cruz Biotechnology, Santa Cruz, CA); anti-HA (Covance Research Products, Denver, PA); anti-phospho-Akt and anti-Akt (Cell Signaling, Danvers, MA). Proteins were visualized by enhanced chemiluminescence (ECL) (Amersham Pharmacia Biotech, Arlington Heights, IL) and quantified by densitometry with Image Master VDS-CL using TINA 2.0 software (Ray Tests).

Fluorescence confocal microscopy

BT-549 stably expressing Gal-3 or Gal-3(V125A) were cultured on cover slips and transfected with GFP-K-RasG12V. Cells were fixed, permeabilized and Gal-3 proteins visualized using rat anti-Gal-3 antibody followed by incubation with biotin-goat anti-rat IgG and Cy3-streptavidin (Jackson ImmunoResearch, West Grove, PA). Confocal analysis as performed using a Zeiss LSM 510 confocal microscope using the appropriate green and red fluorescence filter sets and co-localization was assessed by the co-localization function of the LSM 510 software.

Co-immunoprecipitation and Ras-GTP assays

Co-immunoprecipitation was performed with rabbit anti-Gal-3 antibody and sheep anti-rabbit iron beads (DynaL Biotech, Los Angeles, CA). The beads were collected using a magnetic field and proteins were subjected to Western immunoblotting using the appropriate antibodies. The level of Ras GTP-loading was determined using the glutathione S-transferase- Ras-binding domain of Raf-1 (GST-RBD) pull-down assay as described previously (18) followed by Western immunoblotting with Ras isoform-specific antibodies.

Cell proliferation and FACS analysis

For proliferation assays, 5×10^4 cells/well were plated in 6-well plates. After 4 days phase contrast images were taken and the cells were collected and counted using a haemocytometer. For FACS analysis, 1×10^6 cells were plated per 10cm dish. The following day $10 \mu\text{M}$ adriamycin was added and cells were incubated for 36h. Cells were then collected and re-suspended with PBS containing propidium iodide ($50 \mu\text{g/ml}$) (Sigma) and 0.05% Triton X-100 (BDH, Poole, UK) for DNA staining, then analyzed with a fluorescence-activated cell sorter (FACS Caliber, Becton Dickinson).

Anchorage independent cell growth

For anchorage independent growth assays, 200 cells were suspended in 50ml DMEM containing 10% fetal calf serum (FCS) and 0.5% agarose. The cell suspension was layered on the top of 50ml DMEM containing 10% fetal calf serum (FCS) and 1% soft agarose that had been allowed to gel previously in 96 well plates. The plates were incubated at 37°C for approximately 3 weeks. To visualize colonies, $25 \mu\text{l}$ MTT was added for 4 h and colonies were counted as detailed previously (13).

Electron Microscopy and Statistical analysis

Plasma membrane sheets were prepared, fixed and labelled with affinity purified anti-GFP or anti-mRFP anti-sera coupled directly to 5nm gold as described previously (6,20). For bivariate analysis plasma membrane sheets were labelled sequentially with anti-mRFP (2nm gold) and

anti-GFP (6nm gold) antibodies. Digital images of the immunogold labelled plasma membrane sheets were taken in a transmission electron microscope (Joel 1011). Intact $1\mu\text{m}^2$ areas of the plasma membrane sheet were identified using Image J and the (x,y) coordinates of the gold particles determined as described (6,20). Ripley's K-function (21,22) was calculated using the (x,y) coordinates and then standardized on the 99% confidence interval (CI) for a random pattern (6,20). Bootstrap tests to examine differences between replicated point patterns were constructed exactly as described (23) and statistical significance evaluated against 1000 bootstrap samples.

Fluorescence lifetime imaging- fluorescence resonance energy transfer (FLIM-FRET) microscopy

FLIM experiments were carried out using a lifetime fluorescence imaging attachment (Lambert Instruments, Leutingewolde, The Netherlands) on an inverted microscope (Olympus IX71). BHK cells transiently expressing either mGFP-K-Ras or mGFP-K-RasG12V (donor), alone or with mRFP-Gal-3 (acceptor) (using a 1:3 ratio of plasmid DNA) were excited using a sinusoidally modulated 3W 470nm LED at 80MHz under epi-illumination. Fluorescein was used as a lifetime reference standard. Cells were imaged with a 60x NA 1.45 oil objective using an appropriate GFP filter set. The phase and modulation were determined from a set of 12 phase settings using the manufacturer's software. Resolution of two lifetimes in the frequency domain was performed using a graphical method (24) mathematically identical to global analysis algorithms (25,26). The analysis yields the mGFP lifetime of free mGFP donor ($=\tau_1$), the mGFP lifetime in donor acceptor complexes ($=\tau_2$), and estimates the fraction of mGFP in donor:acceptor complexes (α). Analysis was performed on a cell-by-cell basis. Average FRET efficiency ($=1-\tau_2/\tau_1$) was $53.4 \pm 1.35\%$ (mean \pm s.e.m). To quantify the fraction of mRFP without a functional chromophore we performed FLIM measurements on BHK cells expressing an mGFP-mRFP fusion protein and obtained a value of $\alpha = 0.55 \pm 0.05$ (mean \pm s.e.m). Our estimates of FRET fraction take this into account.

Results

Gal-3 is required for K-Ras.GTP nanocluster formation

The interaction of Gal-3 with K-Ras is GTP-dependent and regulates signal output (12). These characteristics suggest that Gal-3 might operate as a scaffolding protein for K-Ras signalling nanoclusters in a manner analogous to Gal-1 in H-Ras.GTP nanocluster formation (17). To test this hypothesis, we first determined whether Gal-3 is recruited to plasma membrane nanoclusters by K-Ras.GTP. We prepared intact plasma membrane sheets from BHK cells expressing mRFP-Gal-3 alone, or co-expressed with mGFP-K-RasG12V, which is constitutively GTP-loaded, or wild-type mGFP-K-Ras, which is $>95\%$ GDP-loaded in serum starved conditions. The sheets were labelled with anti-mRFP conjugated to 5nm gold. Spatial analysis of the immuno-gold point pattern visualized by EM revealed that expression of mGFP-K-Ras.GTP resulted in increased recruitment of mRFP-Gal-3 to the plasma membrane and that the recruited mRFP-Gal-3 was clustered (Fig. 1A). No recruitment of mRFP-Gal-3 was seen in serum-starved cells expressing wild type mGFP-K-Ras.GDP (Fig. 1A). The clustering characteristics of the mRFP-Gal-3 point pattern on the plasma membrane were similar to that of mGFP-K-RasG12V (Fig. 1B) suggesting that the two proteins may co-localize. The specific interaction between K-RasG12V and Gal-3 was further analyzed in whole cells by FLIM-FRET microscopy. Fig. 1C shows that co-expression of mGFP-K-RasG12V with mRFP-Gal-3, resulted in a significant decrease in the fluorescence lifetime of donor fluorophore (mGFP) suggesting a high degree of molecular interaction between mGFP-K-RasG12V and the acceptor fluorophore (mRFP) tagged Gal-3 (Fig. 1C). Much smaller changes in fluorescence lifetime were observed when wild-type mGFP-K-Ras and mRFP-Gal-3 were co-expressed demonstrating that to bind Gal-3, K-Ras must be GTP-loaded. Taken together these data

suggested that Gal-3 could be a structural element of the K-Ras.GTP nanocluster. To formally test this hypothesis plasma membrane sheets generated from cells expressing mGFP-K-RasG12V and mRFP-Gal-3 were co-labelled with anti-RFP 2nm gold and anti-GFP 6nm gold. Bivariate analysis of the resulting gold point patterns showed that mRFP-Gal-3 and mGFP-K-Ras.GTP co-cluster on the plasma membrane (Fig. 1D). To determine whether Gal-3 is essential for K-Ras nanoclustering, plasma membrane sheets were prepared from cells expressing mGFP-K-RasG12V that were replete or depleted of Gal-3, and labelled with anti-GFP-5nm gold. Spatial analysis of the resulting gold pattern showed that K-Ras.GTP nanoclustering was significantly decreased in cells that had reduced levels of cytosolic Gal-3 (Fig. 1B), mGFP-K-Ras nanoclustering was not decreased in similar experiments (data not shown). Importantly spatial analysis of plasma membrane sheets derived from cells co-expressing mGFP-K-RasG12V and an anti-sense Gal-1 construct or treated with β -lactose, a competitive inhibitor of Gal-3 binding at the cell surface, demonstrated that K-Ras.GTP nanocluster formation was not affected (data not shown). Taken together these data demonstrate that Gal-3 acts specifically as a scaffold for the formation of the K-Ras.GTP but not the K-Ras.GDP nanocluster, demonstrating for the first time that K-Ras forms distinct nanoclusters depending upon the bound nucleotide.

The cytoplasmic concentration of Gal-3 modulates the level of K-Ras nanocluster formation

The results in Fig. 1 predict that the clustered fraction of K-Ras.GTP is determined by the cytosolic concentration of Gal-3. To directly test this prediction we varied Gal-3 levels by ectopically expressing mRFP-Gal-3 (12). We prepared, and immuno-gold labelled, intact plasma membrane sheets from BHK cells expressing mGFP-K-RasG12V, alone or co-expressed with different ratios of mRFP-Gal-3. The spatial analysis of the anti-GFP gold labelling revealed that the level of K-Ras.GTP clustering increased in proportion to the increased Gal-3 expression levels (Fig. 2A). The spatial analysis of the anti-mRFP gold labelling demonstrated the increased K-RasG12V nanocluster formation was associated with a concomitant increase in mRFP-Gal-3 nanoclustering without any increase in nanocluster radius (Fig. 2B).

V125 in Gal-3 is the structural homologue to L11 in Gal-1

Taken together the results in Figures 1 and 2 show that Gal-3 is an integral component of the K-Ras.GTP nanocluster and directly regulates the K-Ras.GTP clustered fraction. We have shown previously that the K-Ras-Gal-3 interaction is dependent on K-Ras prenylation as with H-Ras and Gal-1 (12, 14). To identify the putative prenyl binding pocket of Gal-3, we performed sequence and structure alignments on Gal-1 and Gal-3. Although the sequences of Gal-1 and Gal-3 were not highly conserved (Fig. 3A) the structures of the CRD domains of Gal-3 and Gal-1 (respective PDB codes 1SLA and 1A3K) are remarkably similar (Fig. 3B). Moreover our alignment showed that L11, which lies in the prenyl-binding pocket of Gal-1 and regulates interaction between Gal-1 and H-Ras, is structurally equivalent to V125 in Gal-3 (Fig. 3B). We speculated that mutation of valine 125 to alanine may interfere with the functions of K-Ras in a manner analogous to the dominant negative action of Gal-1(L11A) on H-Ras.GTP (14). Fig. 4A shows that recombinant wild-type Gal-3 and Gal-3(V125A) both bound to a lactosylated Sepharose 4B column and exhibited an almost identical elution pattern with lactose. This result indicates that the V125A substitution does not cause a major distortion of the carbohydrate-binding capacity of Gal-3 and that the mutant protein is properly folded.

Gal-3 (V125A) interacts with active K-Ras

To determine whether the V125A mutation affects the ability of Gal-3 to regulate K-Ras activity, we first tested whether Gal-3(V125A) can interact directly with K-Ras.GTP in a manner analogous to wild-type Gal-3 (12,13). Co-immunoprecipitation studies were

performed on cell lysates generated from cells co-expressing GFP-K-RasG12V with either Gal-3 or Gal-3(V125A). In line with previous studies (12,13), Gal-3 co-immunoprecipitated with GFP-K-RasG12V (Fig. 4B). Importantly, the Gal-3(V125A) mutant also co-immunoprecipitated with K-RasG12V (Fig. 4B) suggesting that the V125A mutation does not affect the ability of Gal-3 to interact with K-Ras.GTP.

Gal-3 and K-Ras.GTP co-localize at the plasma membrane. Therefore we next explored whether the V125A mutation altered the subcellular distribution of Gal-3 and K-Ras.GTP (12,13). Cells expressing GFP-K-RasG12V with either Gal-3 or Gal-3(V125A) were analyzed by immunofluorescence. We detected significant co-localization between GFP-K-RasG12V and Gal-3 at the plasma membrane (Fig. 4C). However, when we co-expressed K-RasG12V with Gal-3(V125A) in addition to plasma membrane co-localization, we also detected significant co-localization between GFP-K-RasG12V and Gal-3(V125A) in the cytosol and intracellular compartments (Fig. 4C). Together these data suggest that Gal-3(V125A) interacts with K-Ras and may reduce K-Ras association with the plasma membrane.

Gal-3(V125A) abrogates K-Ras nanocluster formation

We next examined whether Gal-3(V125A) would interfere with K-Ras.GTP nanocluster formation. We used immuno-EM to analyze the spatial distribution of K-Ras.GTP in the presence or absence of Gal-3(V125A). Fig. 4D shows that co-expression of K-RasG12V with Gal-3(V125A) resulted in a significant decrease in the level of K-Ras.GTP nanocluster formation compared to control cells. In contrast, co-expression of Gal-3(V125A) with K-Ras.GDP did not alter nanocluster formation (data not shown). These data are entirely consistent with those in Fig. 1 demonstrating the Gal-3 is specifically required for K-Ras.GTP but not K-Ras.GDP nanocluster formation.

Gal-3(V125A) attenuates EGF-stimulated Ras signaling and inhibits activation of GFP-K-Ras

The formation of K-Ras.GTP nanoclusters is essential for signal output since nanoclusters are the sites of effector recruitment (10). Therefore since Gal-3(V125A) reduces K-Ras.GTP nanoclustering, Gal-3(V125A) would be expected to inhibit K-Ras signal output. We compared the impact of Gal-3 and Gal-3(V125A) on Ras signaling via the Raf/MEK/ERK signaling pathway. Consistent with previous experiments (13,27) and its role in regulating K-Ras.GTP nanocluster formation (Fig. 1), Gal-3 expression in BT-549 cells caused a significant increase in phospho-ERK levels (Fig. 5A). By marked contrast Gal-3(V125A) caused a significant decrease in phospho-ERK levels in all three BT-549/Gal-3(V125A) clones (Fig. 5A). Thus, compared with BT-549 cells BT-549/Gal-3(V125A) cells exhibit attenuated Ras/Raf/MEK/ERK signaling consistent with the associated decrease in K-Ras.GTP nanocluster formation.

We next examined the effect of Gal-3(V125A) on epidermal growth factor (EGF)-stimulated GTP-loading of K-Ras in HEK 293 cells. In control cells, EGF induced a transient increase in K-Ras GTP-loading (Fig. 5B). In comparison, in cells co-expressing GFP-K-Ras and Gal-3 (V125A) EGF-stimulated significantly less K-Ras GTP-loading (Fig. 5A). These data suggest that Gal-3(V125A) inhibits K-Ras activation. Similar findings were observed in three distinct clones of the breast cancer cell line BT-549 stably expressing Gal-3(V125A). BT-549 cells express low levels of Gal-3 (13,28) and stable expression of Gal-3 in BT-549 cells increases the levels of K-Ras.GTP (13). In contrast, the levels of K-Ras.GTP in all three BT-549/Gal-3 (V125A) clones were significantly lower than those recorded in BT-549 cells and BT-549 cells expressing Gal-3 (Fig. 5B). K-Ras expression was also somewhat lower in the BT-549/Gal-3 (V125A) clones compared with the parental BT-549 cells, suggesting that Gal-3(V125A) may decrease K-Ras protein stability and/or expression. These results are in line with the observed inhibition of the EGF-stimulated K-Ras GTP-loading by Gal-3(V125A) in HEK 293 cells (Fig. 5B).

Gal-3(V125A) reverses the transformed phenotype of BT-549 cells

To further explore the capacity of Gal-3(V125A) to inhibit K-Ras signaling we measured the effect of Gal-3(V125A) on BT-549 cell proliferation. BT-549, BT-549/ Gal-3 and BT-549/ Gal-3(V125A) were plated at equal densities and cell numbers were counted after four days. Phase-contrast imaging and cell counting confirmed that proliferation was compromised in BT-549 Gal-3(V125A) compared to the other cell lines analyzed; the rank order of cell number recorded was BT-549/ Gal-3 > BT-549 > BT-549/ Gal-3(V125A) (Fig. 6A and 6B).

Ras signaling causes resistance to cytotoxic drug induced cell death in BT-549/Gal-3 cells compared to parental BT-549 cells (13,27,29). Therefore we compared the sensitivity of BT-549, BT-549/Gal-3 and BT-549/ Gal-3(V125A) cells to adriamycin by FACS analysis. Adriamycin induced an increase in the sub-G1 population of cells (indicative of apoptotic cell death) in BT-549 cells and in all BT-549/ Gal-3(V125A) cell lines but not in BT-549/Gal-3 cells which were highly resistant (Fig. 6C). The increase in sub-G1 population observed in all BT-549/ Gal-3(V125A) cell lines was clearly higher than that observed in BT-549 cells (Fig. 6C) suggesting that Gal-3(V125A) had rendered the cells more sensitive to apoptosis.

Finally, we examined the effect of Gal-3(V125A) on the anchorage-independent growth of BT-549 cells. We found that BT-549/Gal-3 cells formed a relatively high number of large colonies, BT-549 cells formed an intermediate number of colonies and BT-549/Gal-3(V125A) cells formed a limited number of small colonies that were reduced in size compared to BT-549 cells (Fig. 6D). Thus the transformed phenotype of BT-549 cells was partially reversed by the introduction of Gal-3(V125A).

Discussion

A plethora of control mechanisms exist in mammalian cells to regulate the initiation, duration and magnitude of intracellular signal transduction. Malfunction of these control mechanisms results in tumor formation. One recently discovered level of control is provided by the spatial organisation of Ras proteins on the plasma membrane. Approximately, 40% of Ras proteins are organised into nanoclusters. Importantly only Ras proteins resident in nanoclusters can recruit effectors and initiate signal transduction (10). Ras nanoclusters function as transient nanoscale digital switches capable of transducing signal with high-fidelity (6,7,10). Here we investigate the mechanisms that regulate K-Ras.GTP nanoclustering. We demonstrate through the use of immuno-EM spatial mapping and FLIM-FRET microscopy that Gal-3 directly controls K-Ras.GTP but not K-Ras.GDP nanocluster formation and function. Our data show that Gal-3 is a structural component of the K-Ras.GTP nanocluster and that the cytosolic pool of Gal-3 available for recruitment is the critical determinant of the K-Ras.GTP clustered fraction. Through structural modeling we identified a mutant of Gal-3 that effectively abrogates K-Ras.GTP nanoclustering, inhibiting signal transduction and transformation.

An important implication of these results is that K-Ras undergoes nucleotide-dependent lateral segregation on the inner leaflet of the plasma membrane as previously shown for H-Ras (6, 30,31). In the inactive GDP-conformation, K-Ras resides in Gal-3-independent nanoclusters and Gal-3 is localised predominantly to the cytoplasm. Following K-Ras GTP-loading Gal-3 is recruited from the cytoplasm to the plasma membrane. Exactly how Gal-3 recognises the GTP-bound form of K-Ras is currently unknown. However we speculate that the interaction between Gal-3 and K-Ras.GTP may occur in a manner analogous to the interaction of RhoGDI's with their cognate GTPases (reviewed in (32)). If so Gal-3 would recognise GTP-dependent conformational changes in the K-Ras switch I and switch II regions by directly contacting the K-Ras G-domain. Indeed Gal-3(V125A), which contains a mutation in the putative prenyl-binding pocket, retains the ability to sense the GTP form of K-Ras. This result suggests the

presence of additional interaction sites which might include the previously identified Gal-3 residues S6 and G182 that are known to be critical for interaction with K-Ras (13).

Sequestration of the farnesyl group into the Gal-3 hydrophobic pocket might be expected to decrease K-Ras membrane affinity. However, Gal-3 has been shown to bind to lipids including phosphatidylserine in *in vitro* assays (33). Therefore Gal-3 might compensate for the loss of membrane affinity following sequestration of the farnesyl group by interacting directly with the lipid bilayer. Thus GTP-loading and interaction with Gal-3 will decrease the dissociation rate of K-Ras from the plasma membrane increasing K-Ras membrane association as detected by immuno-EM. An additional gain in membrane affinity may flow from the ability of Gal-3 molecules to form higher order oligomers such as pentamers and hexamers through homotypic N-terminal interactions (34,35).

The Gal-3(V125A) mutant does not provide K-Ras.GTP with additional membrane affinity. Indeed interaction with Gal-3(V125A) leads to extraction of K-Ras from the plasma membrane. In context of the model proposed above this may reflect a failure of Gal-3(V125A) to provide a functioning scaffold for the formation of the K-Ras.GTP nanoclusters; either by directly destabilizing K-Ras.GTP membrane interaction, or indirectly by preventing Gal-3 oligomerisation. Alternatively mutation of valine 125 to alanine may reduce Gal-3 lipid binding affinity (7). Whatever the precise mechanism our data clearly demonstrate that the ability of Gal-3 to act as a positive regulator of K-Ras.GTP nanocluster formation and function is finely tuned since only small changes within the Gal-3 protein are sufficient to turn Gal-3 into a potent inhibitor. Taken together these data suggest that a K-Ras.GTP-Gal-3 complex is the basic building block of the K-Ras.GTP nanocluster which is then assembled into a larger structure by Gal-3 protein-protein interactions. The clustering of ~7 K-Ras.GTP proteins will increase the local concentration of acidic phospholipids further stabilising the nanocluster via electrostatic interaction.

Increased nanoclustering induced by ectopic Gal-3 expression correlates with increased K-Ras.GTP levels. In the context of previous studies showing that exogenous Gal-3 expression effectively decreases p120RasGAP activity (12) our new results suggest that K-Ras.GTP proteins resident in nanoclusters may be relatively inaccessible to p120RasGAP perhaps due to conformational or spatial constraints imposed by the nanocluster.

Taken together these data show that the availability of Gal-3 in the cytosol for recruitment by K-Ras.GTP is the critical determinant of the fraction K-Ras.GTP proteins that reside in nanoclusters compared to those that exist as monomers on the inner plasma membrane. The K-Ras.GTP clustered fraction is a key parameter, which sets the sensitivity of EGF dependent activation of the MAPK cascade (10). Our new data now implicate the cytosolic pool of Gal-3 as a modulator of MAPK activation by EGF and oncogenic mutant K-RasG12V. This finding has important implications because Gal-3 expression is altered in a number of tumour types in turn increasing the cytosolic pool of Gal-3 available for K-RasG12V interaction (27,36). Gal-3 has been implicated in neoplastic progression and metastasis (reviewed in (11)). Our model predicts that the increased availability of cytosolic Gal-3 will increase the K-RasG12V clustered fraction. Since downstream effectors are recruited only by K-RasG12V proteins resident in nanoclusters (10), resetting the ratio of clustered fraction to monomer will lead to increased effector recruitment and activation, the net result being an increased level of signal output from the same number of K-RasG12V proteins. Furthermore, over-expression of Gal-3 in the absence of oncogenic K-Ras mutations will facilitate increased signal output via K-Ras in response to a normal level of growth factor stimulation leading to aberrant cellular behaviour and potentially tumour formation (12,13). In conclusion, we suggest that K-Ras mutational activation and/or increased Gal-3 expression may co-operate to drive tumorigenesis via the

constitutive activation of the Raf/MEK/ERK pathway. Thus Gal-3 over-expression represents the first example of an oncogenic mechanism that subverts membrane nanostructure.

Acknowledgments

This work was supported in part by grant 2005344 from the United States–Israel Binational Science Foundation (BSF), The Wolfson Family Foundation (Y.K) and the National Health and Medical Research Council (Australia) and the NIH (GM066717) (JFH). Yoel Kloog is the incumbent of The Jack H. Skirball Chair for Applied Neurobiology. IMB is a Special Research Centre of the ARC. We thank S.R. Smith for editorial assistance.

References

1. Cox AD, Der CJ. The dark side of Ras: regulation of apoptosis. *Oncogene* 2003;22:8999–9006. [PubMed: 14663478]
2. Downward J. Targeting RAS signalling pathways in cancer therapy. *Nat Rev Cancer* 2003;3:11–22. [PubMed: 12509763]
3. Mitin N, Rossman KL, Der CJ. Signaling interplay in Ras superfamily function. *Curr Biol* 2005;15:563–74.
4. Bos JL. ras oncogenes in human cancer: a review. *Cancer Res* 1989;49:4682–9. [PubMed: 2547513]
5. Hancock JF. Ras proteins: different signals from different locations. *Nat Rev Mol Cell Biol* 2003;4:373–84. [PubMed: 12728271]
6. Prior IA, Muncke C, Parton RG, Hancock JF. Direct visualization of Ras proteins in spatially distinct cell surface microdomains. *J Cell Biol* 2003;160:165–70. [PubMed: 12527752]
7. Plowman SJ, Muncke C, Parton RG, Hancock JF. H-ras, K-ras, and inner plasma membrane raft proteins operate in nanoclusters with differential dependence on the actin cytoskeleton. *Proc Natl Acad Sci U S A* 2005;102:15500–5. [PubMed: 16223883]
8. Hancock JF, Parton RG. Ras plasma membrane signalling platforms. *Biochem J* 2005;389:1–11. [PubMed: 15954863]
9. Murakoshi H, Iino R, Kobayashi T, et al. Single-molecule imaging analysis of Ras activation in living cells. *Proc Natl Acad Sci U S A* 2004;101:7317–22. [PubMed: 15123831]
10. Tian T, Harding A, Inder K, Plowman S, Parton RG, Hancock JF. Plasma membrane nanoswitches generate high-fidelity Ras signal transduction. *Nat Cell Biol* 2007;9:905–14. [PubMed: 17618274]
11. Dumic J, Dabelic S, Fogel M. Galectin-3: an open-ended story. *Biochim Biophys Acta* 2006;1760:616–35. [PubMed: 16478649]
12. Elad-Sfadia G, Haklai R, Balan E, Kloog Y. Galectin-3 augments K-Ras activation and triggers a Ras signal that attenuates ERK but not phosphoinositide 3-kinase activity. *J Biol Chem* 2004;279:34922–30. [PubMed: 15205467]
13. Shalom-Feuerstein R, Cooks T, Raz A, Kloog Y. Galectin-3 regulates a molecular switch from N-Ras to K-Ras usage in human breast carcinoma cells. *Cancer Res* 2005;65:7292–300. [PubMed: 16103080]
14. Rotblat B, Niv H, Andre S, Kaltner H, Gabius HJ, Kloog Y. Galectin-1(L11A) predicted from a computed galectin-1 farnesyl-binding pocket selectively inhibits Ras-GTP. *Cancer Res* 2004;64:3112–8. [PubMed: 15126348]
15. Paz A, Haklai R, Elad-Sfadia G, Ballan E, Kloog Y. Galectin-1 binds oncogenic H-Ras to mediate Ras membrane anchorage and cell transformation. *Oncogene* 2001;20:7486–93. [PubMed: 11709720]
16. Ashery U, Yizhar O, Rotblat B, et al. Spatiotemporal Organization of Ras Signaling: Rasosomes and the Galectin Switch. *Cellular and Molecular Neurobiology* 2006;26:469–93.
17. Belanis L, Plowman SJ, Rotblat B, Hancock JF, Kloog Y. Galectin-1 Is a Novel Structural Component and a Major Regulator of H-Ras Nanoclusters. *Mol Biol Cell*. 2008
18. Elad-Sfadia G, Haklai R, Ballan E, Gabius HJ, Kloog Y. Galectin-1 augments Ras activation and diverts Ras signals to Raf-1 at the expense of phosphoinositide 3-kinase. *J Biol Chem* 2002;277:37169–75. [PubMed: 12149263]

19. Campbell RE, Tour O, Palmer AE, et al. A monomeric red fluorescent protein. *Proc Natl Acad Sci U S A* 2002;99:7877–82. [PubMed: 12060735]
20. Hancock JF, Prior IA. Electron microscopic imaging of Ras signaling domains. *Methods* 2005;37:165–72. [PubMed: 16288888]
21. Besag JE. Contribution to the discussion of Dr. Ripley's paper. *J R Statist Soc* 1977;39:193–5.
22. Ripley BD. Modelling spatial patterns. *J R Statist Soc* 1977;39:172–92.
23. Diggle PJ, Mateu J, Clough HE. A comparison between parametric and non-parametric approaches to the analysis of replicated spatial point patterns. *Adv Appl Prob (SGSA)* 2000;32:331–43.
24. Clayton AH, Hanley QS, Verveer PJ. Graphical representation and multicomponent analysis of single-frequency fluorescence lifetime imaging microscopy data. *J Microsc* 2004;213:1–5. [PubMed: 14678506]
25. Esposito A, Gerritsen HC, Wouters FS. Fluorescence lifetime heterogeneity resolution in the frequency domain by lifetime moments analysis. *Biophys J* 2005;89:4286–99. [PubMed: 16169974]
26. Verveer PJ, Bastiaens PI. Evaluation of global analysis algorithms for single frequency fluorescence lifetime imaging microscopy data. *J Microsc* 2003;209:1–7. [PubMed: 12535178]
27. Takenaka Y, Fukumori T, Yoshii T, et al. Nuclear export of phosphorylated galectin-3 regulates its antiapoptotic activity in response to chemotherapeutic drugs. *Mol Cell Biol* 2004;24:4395–406. [PubMed: 15121858]
28. Gong HC, Honjo Y, Nangia-Makker P, et al. The NH2 terminus of galectin-3 governs cellular compartmentalization and functions in cancer cells. *Cancer Res* 1999;59:6239–45. [PubMed: 10626818]
29. Yoshii T, Fukumori T, Honjo Y, Inohara H, Kim HR, Raz A. Galectin-3 phosphorylation is required for its anti-apoptotic function and cell cycle arrest. *J Biol Chem* 2002;277:6852–7. [PubMed: 11724777]
30. Rotblat B, Prior IA, Muncke C, et al. Three separable domains regulate GTP-dependent association of H-ras with the plasma membrane. *Mol Cell Biol* 2004;24:6799–810. [PubMed: 15254246]
31. Roy S, Plowman S, Rotblat B, et al. Individual palmitoyl residues serve distinct roles in h-ras trafficking, microlocalization, and signaling. *Mol Cell Biol* 2005;25:6722–33. [PubMed: 16024806]
32. Dovas A, Couchman JR. RhoGDI: multiple functions in the regulation of Rho family GTPase activities. *Biochem J* 2005;390:1–9. [PubMed: 16083425]
33. Lukyanov P, Furtak V, Ochieng J. Galectin-3 interacts with membrane lipids and penetrates the lipid bilayer. *Biochem Biophys Res Commun* 2005;338:1031–6. [PubMed: 16248982]
34. Mehul B, Bawumia S, Hughes RC. Cross-linking of galectin 3, a galactose-binding protein of mammalian cells, by tissue-type transglutaminase. *FEBS Lett* 1995;360:160–4. [PubMed: 7875321]
35. Ahmad N, Gabius HJ, Andre S, et al. Galectin-3 precipitates as a pentamer with synthetic multivalent carbohydrates and forms heterogeneous cross-linked complexes. *J Biol Chem* 2004;279:10841–7. [PubMed: 14672941]
36. Califice S, Castronovo V, Van Den Brule F. Galectin-3 and cancer (Review). *Int J Oncol* 2004;25:983–92. [PubMed: 15375548]

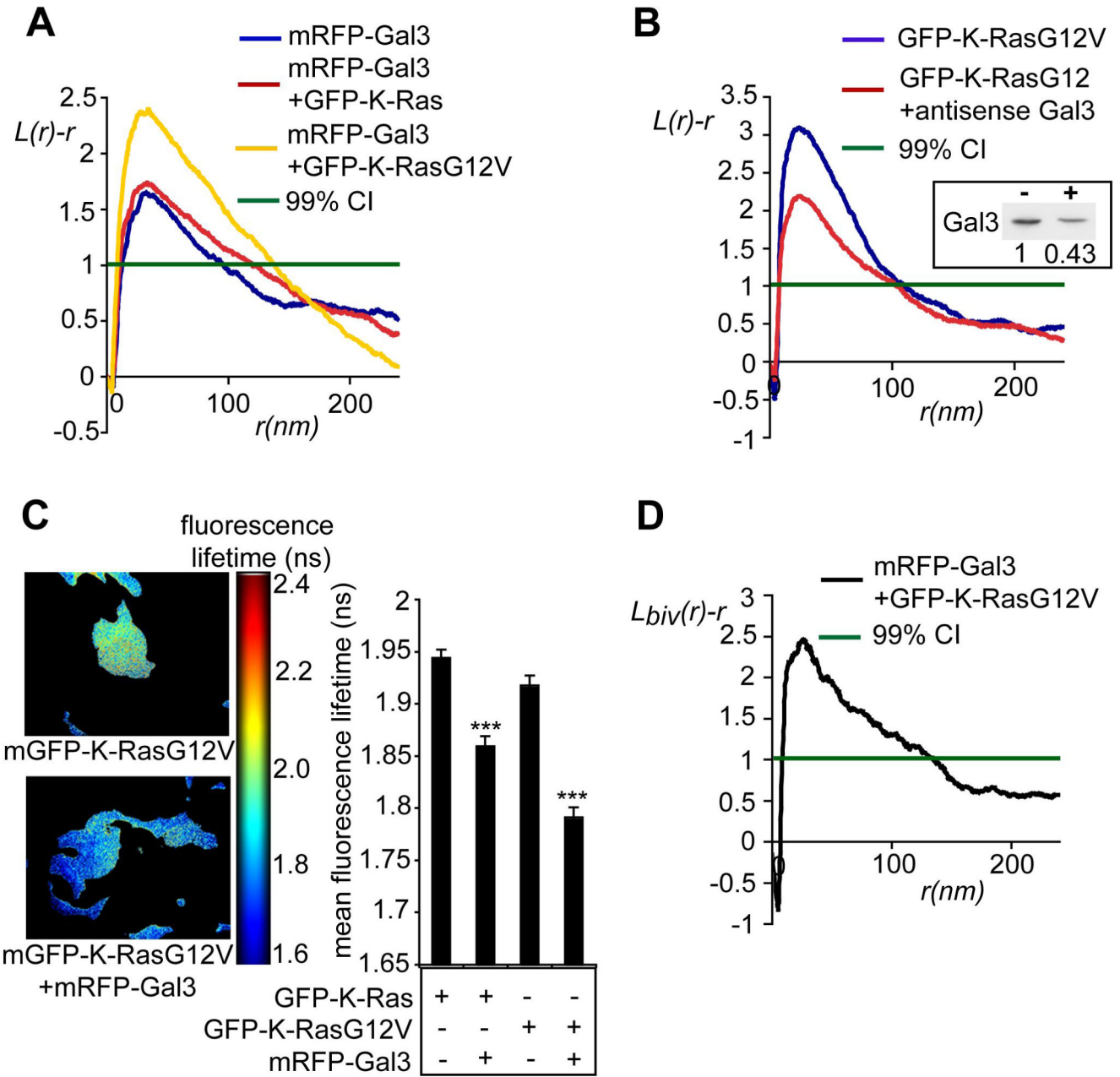


Figure 1. Gal-3 is a structural component of K-Ras nanoclusters on the plasma membrane

A, Plasma membrane sheets were prepared from cells expressing mRFP-Gal-3 in the presence or absence of mGFP-K-Ras or mGFP-K-RasG12V. Sheets were labelled with anti-mRFP antibodies conjugated to 5nm gold. The spatial distribution of the resulting gold patterns were analyzed. K-functions are weighted means ($n \geq 8$) standardized on the 99% CI for a random pattern. Significance differences from control patterns were assessed using bootstrap tests. Co-expression of mGFP-K-Ras with mRFP-Gal-3 did not significantly alter the basal level of Gal-3 nanoclustering detected in the absence of exogenous K-Ras expression ($p=1$). However co-expression of mRFP-Gal-3 with mGFP-K-RasG12V resulted in a significant increase in Gal-3 nanocluster formation ($p=0.001$), which was associated with a significant increase in Gal-3 plasma membrane localisation (number of gold particles/ $\mu\text{m}^2 = 26.3 \pm 3.7$ and 47.9 ± 4.8 respectively, t -test $p=0.002$). **B**, Plasma membrane sheets were prepared from cells expressing

mGFP-K-RasG12V in the presence or absence of a Gal-3 antisense construct. Sheets were labelled with anti-GFP antibodies conjugated to 5nm gold. Significance difference from the control K-RasG12V point pattern was assessed using bootstrap tests. Co-expression of mGFP-K-RasG12V with the antisense Gal-3 construct significantly reduced the level of K-RasG12V nanocluster formation ($p=0.001$). Inset panel: Expression of the antisense Gal-3 construct reduced endogenous Gal-3 level by $\sim 50\%$. *C*, Cells expressing mGFP-K-Ras or mGFP-K-RasG12V, alone, or with mRFP-Gal-3 were imaged in the frequency domain in a wide-field FLIM-FRET microscope. Representative fluorescence lifetime images are shown. The graph represents the mean fluorescence lifetime of mGFP (\pm s.e.m) measured in 22–50 cells. Significant differences from control mGFP-K-RasG12V or mGFP-K-Ras lifetimes were assessed using t-tests (***) $p < 0.0001$). *D*, Co-localization of mRFP-Gal-3 and mGFP-K-RasG12V. Plasma membrane sheets generated from cells expressing mRFP-Gal-3 and mGFP-K-RasG12V were co-labelled with anti-mRFP (2nm gold) and anti-GFP (6nm gold) antibodies. $L_{biv}(r)$ -r curves above the 99% CI for random patterns indicate significant co-localization. The bivariate K-functions are weighted means ($n = 13$) standardized on the 99% CI.

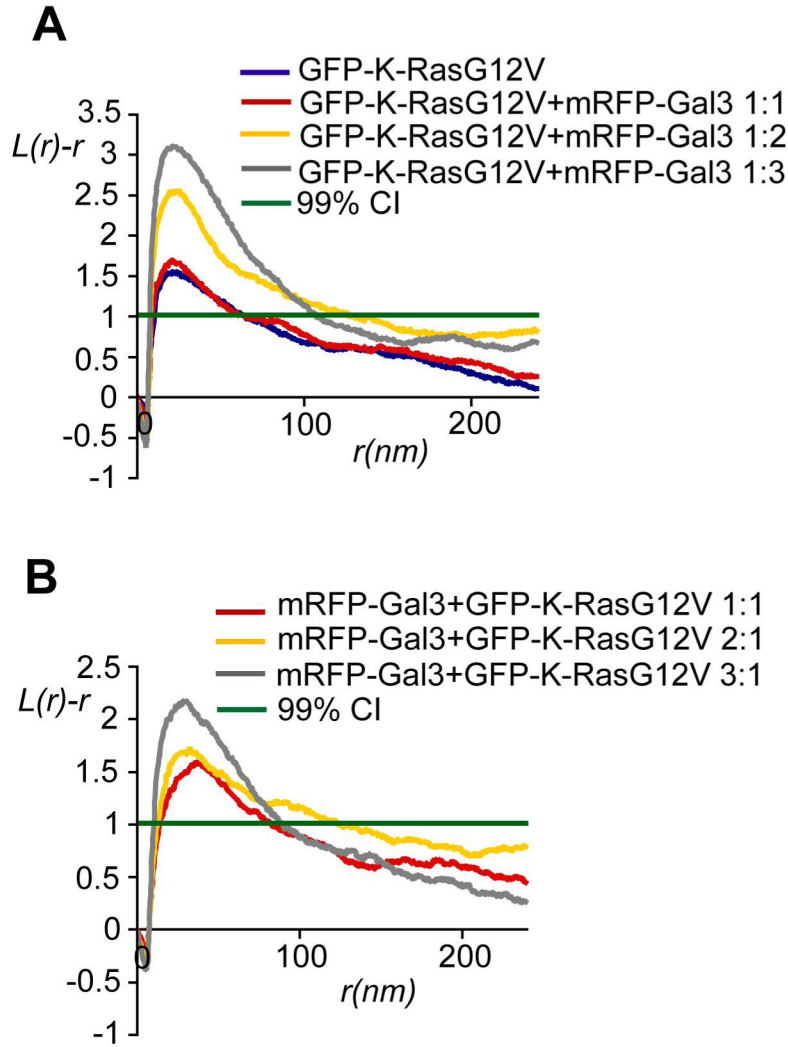


Figure 2. Cytosolic Gal-3 levels regulate the extent of K-Ras nanoclustering on the plasma membrane

Increasing Gal-3 levels increases L_{max} but not $\sup_r |L(r)-r|$ of the K-RasG12V K-function. (A-B) Plasma membrane sheets were prepared from cells expressing GFP-K-RasG12V in the presence or absence of mRFP-Gal-3. The level of GFP-K-RasG12V expression was kept constant, while the ratio of mRFP-Gal-3 expression relative to GFP-K-RasG12V was increased (1:1, 1:2 and 1:3). Sheets were immuno-gold labelled with (A) anti-GFP antibodies or (B) anti-mRFP antibodies and the gold point patterns analyzed. $L(r)-r$ curves are weighted mean K-functions ($n=8-10$). Significant differences from control point patterns were assessed by bootstrap tests. A, Increasing mRFP-Gal-3 expression resulted in a significant increase in GFP-K-RasG12V nanocluster formation ($p=0.001$). B, The increase in GFP-K-RasG12V nanocluster formation was also associated with a significant increase in mRFP-Gal-3 nanoclustering ($p=0.001$)

A

Gal-3	1	ADNFSLHDALSGSGNPNPQGMFGAWGNQPAGAGGYPGASYPGAYPGQAPPGAYPGQAPPG
Gal-1	1
Gal-3	61	AYHGAPGAYPGAPAGVYPGPPSGPGAYPSGQPSAPGAYPATGPGYGAAPAGPLIVPYNLP
Gal-1	1ACG.....LVASNLN
		V125↓
Gal-3	121	LPGGVVPRMLITILGTVKPNANRIALDFQR.GNDVAFHFNPRFEN.NRRVIVCNTKLDN
Gal-1	11	LK...PGECLRVRGEVAPDAKSEVLNLGKDSNNLCLHFNPRFNAHGDANTIVCNSKDGG
		L11↑
Gal-3	179	NWGREERQSVFPFESGKPFKIQVLVEPDHFKVAVND AHL LQYNHRVKKLINEISKLGISGD
Gal-1	67	AWGTEQREAVFPFQPGSVAEVCITFDQANLTVKLPDGYEFKFPNRLN.LEA INYMAADGD
Gal-3	239	IDLTSASYTMI
Gal-1	126	FKIKCVAFD..

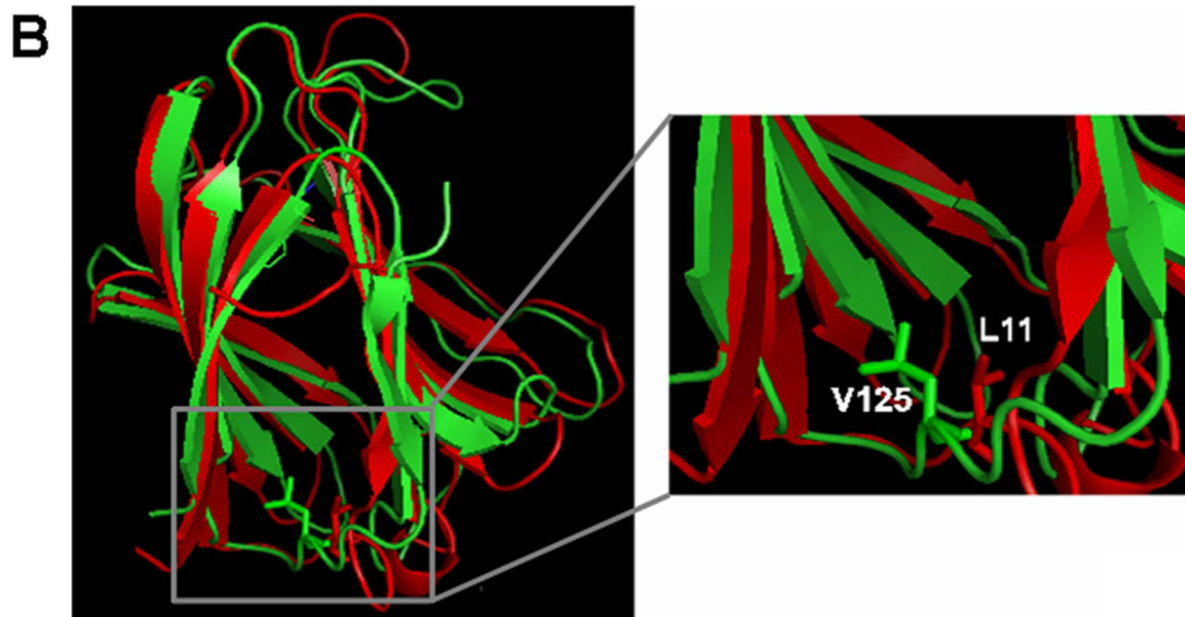


Figure 3. V125 in Gal-3 is the structural homologue to L11 in Gal-1

A, Sequence alignment of human Gal-1 and human Gal-3. Identical amino-acids are shown in red. **B**, The structural superimposition analysis of Gal-1 (red) and the CRD domain of Gal-3 (green) (PDB codes: 1SLA and 1A3K respectively) is presented in the left-hand panel. The right-hand panel is a higher magnification of the region outlined by the grey square in the left-hand panel. Residues L11 and V125 of Gal-1 and Gal-3 respectively are shown in white.

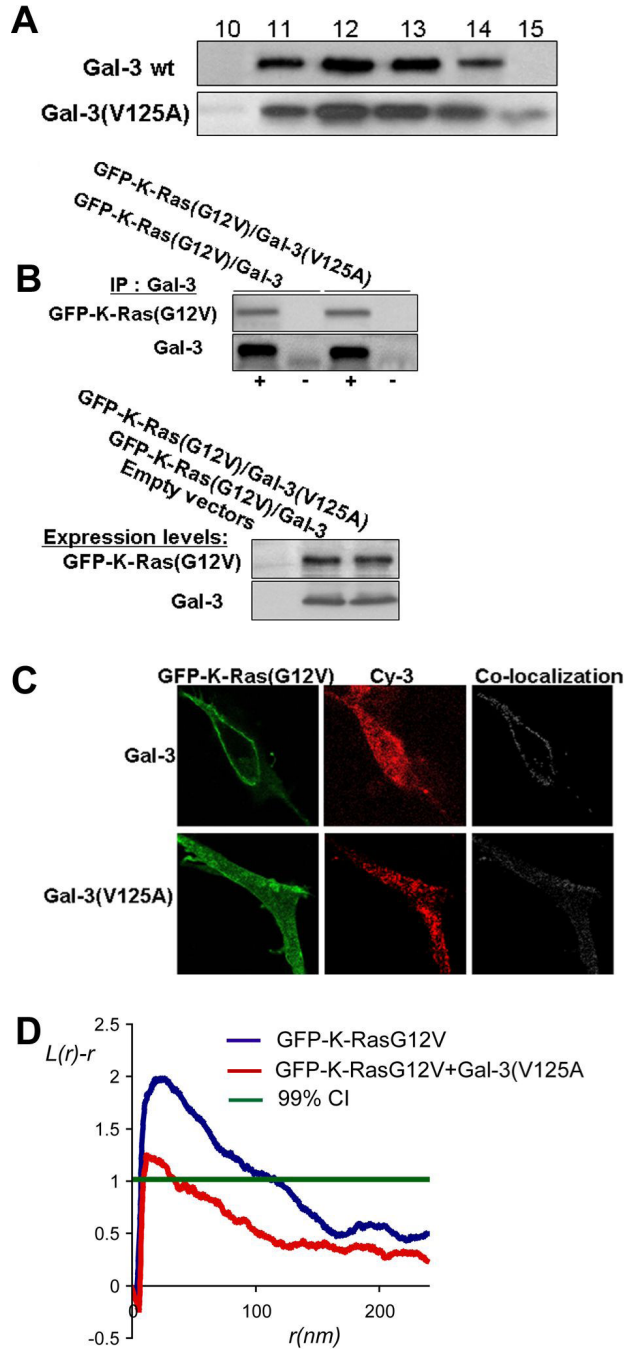


Figure 4. Gal-3(V125A) interacts with and induces mislocalization of GFP-K-RasG12V
 A, Gal-3(V125A) bind to lactosylated Sepharose. Bacterially expressed recombinant Gal-3 or Gal-3(V125A) proteins were loaded onto lactosylated Sepharose column then eluted with lactose. The collected fractions were subjected to immunoblotting with anti-Gal-3 antibody. Blots of the peak fractions are shown. B, Gal-3(V125A) co-immunoprecipitates with GFP-K-RasG12V. Cell lysates were generated from HEK 293 cells co-expressing GFP-K-RasG12V with either Gal-3 or Gal-3(V125A) and subjected to immunoprecipitation (IP) with anti-Gal-3 antibody (+) or with no antibody (-). The immunoprecipitates were then immunoblotted (IB) with anti-Ras or anti-Gal-3 antibodies. Representative immunoblots are shown (n=3). C, Analysis of GFP-K-RasG12V and Gal-3 co-localization by immunofluorescence. BT-549

stably expressing Gal-3 or Gal-3(V125A) were transfected with plasmid DNA encoding for GFP-K-RasG12V. Gal-3 proteins were visualized using an anti-Gal-3 antibody and a Cy-3 conjugated secondary antibody. Cells were imaged by confocal microscopy. Typical images and the extent of co-localization (white) are shown. Note the strong co-localization of Gal-3 and GFP-K-RasG12V at the plasma membrane and the co-localization of Gal-3(V125A) and GFP-K-Ra(G12V in the cytoplasm. Similar images were collected from 10–12 cells. *D*, Gal-3 (V125A) inhibits K-Ras.GTP nanocluster formation. Plasma membrane sheets were prepared from cells expressing GFP-K-RasG12V alone or in the presence of Gal-3(V125A) and labelled with anti-GFP antibodies conjugated to 5nm gold. Significant difference from the control mGFP-K-RasG12V pattern was assessed using a bootstrap test. Co-expression of mGFP-K-RasG12V with Gal-3(V125A) significantly reduced the level of GFP-K-RasG12V nanoclustering compared to the expression of GFP-K-RasG12V alone ($p=0.001$). K-functions are weighted means ($n \geq 7$).

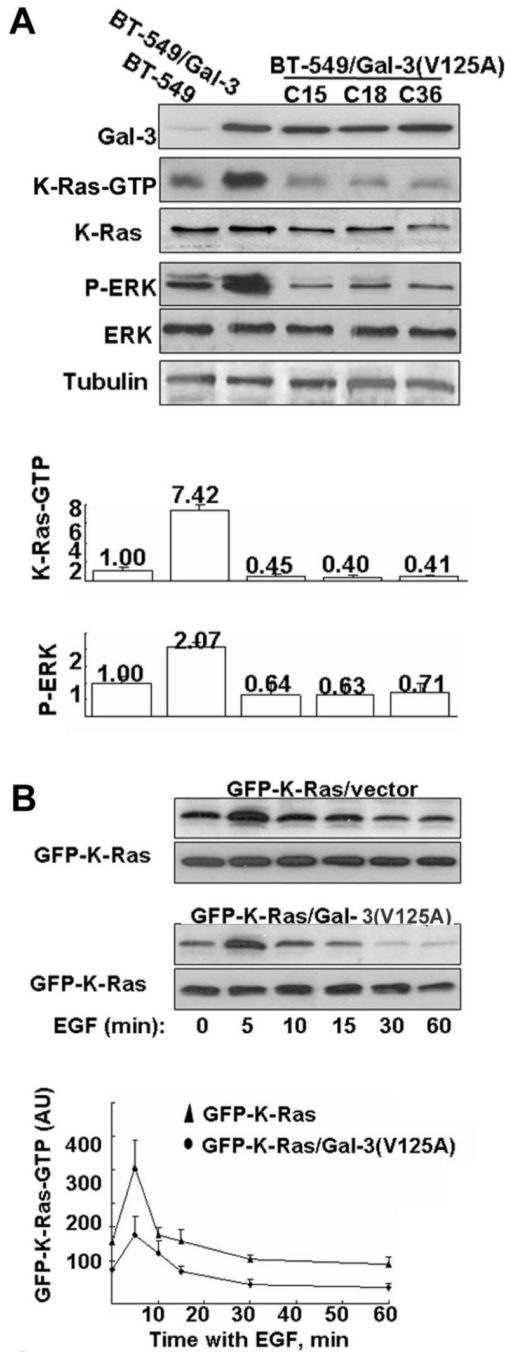


Figure 5. Gal-3(V125A) exhibits dominant negative effects on K-Ras activation

A, Analysis of K-Ras activation and signal transduction in BT-549, BT-549/Gal-3 and BT-549/Gal-3(V125A) cell lines. Representative immunoblots showing Gal-3 and Gal-3(V125A) expression levels and the extent of K-Ras, (K-Ras-GTP) and ERK (P-ERK) activation are shown. Anti β -Tubulin antibody was used as a protein loading control (left-hand panels). The results of densitometry of three independent experiments are presented (right-hand panels). Data are expressed in terms of the ratio of the values recorded in each cell line relative to the values recorded in BT-549 cells (means \pm SD). *B*, Gal-3(V125A) inhibits EGF-stimulated GFP-K-Ras GTP-loading. HEK-293 cells co-transfected with GFP-K-Ras/pcDNA3 (vector control) or GFP-K-Ras/Gal-3(V125A) were serum-starved, and then stimulated with 100 ng/ml EGF

for the indicated times. RBD pull-downs were performed on cell lysates and blots were probed with a pan anti-Ras antibody. Levels of GFP-Ras expression were determined for each sample. Quantification was performed by densitometry. Upper panels: representative immunoblots. Lower panel: results of densitometry (means \pm SD, n = 3) expressed as normalized arbitrary units (AU).

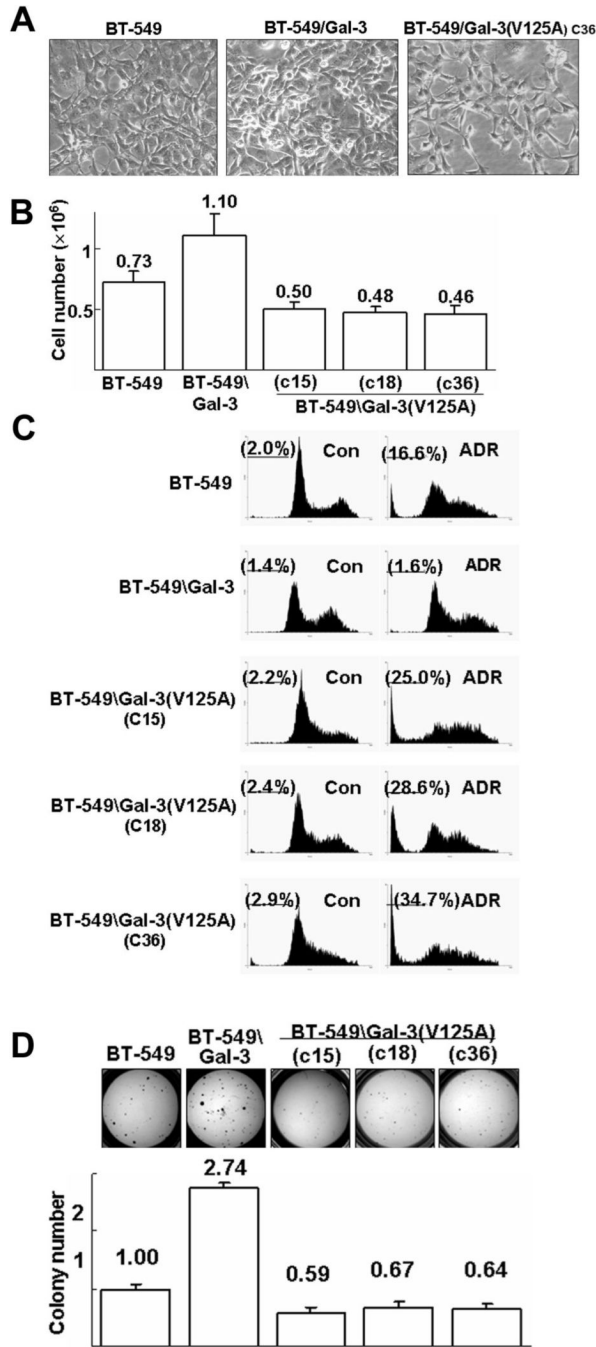


Figure 6. Gal-3(V125A) inhibits BT-549 cell transformation

BT-549/Gal-3(V125A) cells were grown for 4 days in DMEM/10%FCS then imaged under phase-contrast microscope and counted. Typical images of the cells (magnifications $\times 30$) are shown in *A* and results of cell counts (means \pm SD, $n=3$) are shown in *B*. *C*, Gal-3(V125A) increases sensitivity to adriamycin-induced cell death. BT-549, BT-549/Gal-3 and BT-549/Gal-3(V125A) (three distinct clones) cells were treated with 10 μ M adriamycin (ADR) and analyzed 36 h later by FACS. Results of a typical experiment are shown for control (Con) and adriamycin treated cells. The percentage of cells in sub-G1 is denoted in each panel. Similar results were obtained in an additional experiment. *D*, Gal-3(V125A) inhibits anchorage-independent growth of BT-549 cells. Cell lines as indicated in (*A*) were used for soft agar

experiments. Colonies were visualized by MTT staining 21 days after plating (upper panel) and quantified as detailed in Methods. Data are expressed in terms of the number of colonies in each cell line relative to the number of colonies recorded in the BT-549 cultures (mean \pm SD, n=3).